Earth Moon Planets
DOI 10.1007/s11038-011-9385-4

# Lavras do Sul: A New Equilibrated Ordinary L5 Chondrite from Rio Grande do Sul, Brazil

**M. E. Zucolotto · L. L. Antonello · M. E. Varela · R. B. Scorzelli · Isabel P. Ludka · P. Munayco · E. dos Santos**

Received: 4 August 2011 / Accepted: 7 December 2011


**Abstract** The new Brazilian chondrite, Lavras do Sul, was found in 1985 at Lavras do Sul, Rio Grande do Sul State-Brazil (33°30′48″S; 53°54′65″W). It consists of a single mass weighing about 1 kg, covered by a black fusion crust with grayish interior. Four polished thin sections were prepared from a slice weighing 67 g on deposit at the Museu Nacional/UFRJ. It consists mostly of chondrules and chondrule fragments dispersed in a recrystallized matrix. Most chondrules are poorly defined and range in size from 300 to 2,000 μm, although some of them show distinct outlines, particularly when viewed under cross-polarized transmitted and reflected light. The texture of chondrules varies from non-porphyritic (e.g., barred-olivine, radial-pyroxene) to porphyritic ones (e.g., granular olivine as well as olivine-pyroxene). The meteorite contains mainly olivine ($Fa_{24.9}$), low-Ca pyroxene ($Fs_{22.6}$) and metal phases, with minor amounts of plagioclase, chromite and magnetite. Mössbauer Spectroscopy studies indicate that the metal phase is kamacite, tetrataenite and antitaenite. Veins of secondary iddingsite crosscut the thin section and some ferromagnesian silicates. The chemical composition indicates that Lavras do Sul is a member of the low iron L chondrite group. The poorly delineated chondritic texture with few well-defined chondrules, the occurrence of rare clinopyroxene and plagioclase (and maskelynite) with apparent diameters ranging from 5 to 123 μm led us to classify Lavras do Sul as an equilibrated petrologic type 5. The shock features of some minerals suggest a shock stage S3, and the presence of a small amount of secondary minerals such as iddingsite and goethite, a degree of weathering $W_1$. The meteorite name was approved by

M. E. Zucolotto
Museu Nacional/UFRJ, Rio de Janeiro, RJ, Brazil

L. L. Antonello · R. B. Scorzelli (✉) · P. Munayco · E. dos Santos
Centro Brasileiro de Pesquisas Físicas (CBPF/MCT), Rio de Janeiro, RJ, Brazil
e-mail: scorza@cbpf.br

M. E. Varela
ICATE-CONICET, San Juan, Argentina

I. P. Ludka
Instituto de Geociências, UFRJ, Rio de Janeiro, RJ, Brazil

Published online: 09 February 2012

the Nomenclature Committee (Nom Com) of the Meteoritical Society (Meteoritic Bulletin N°99).

**Keywords** Brazilian meteorite · Chondrite · Electron microprobe · Mössbauer spectroscopy

## 1 Introduction

The Lavras do Sul meteorite was found in 1985 by Professor Picada from the Geosciences Institute/UFRGS, in a stream pebble field bed in the vicinity of Lavras do Sul, Rio Grande do Sul State, Brazil. It is a single stone of about 1 kg, with mean dimensions of 10 × 5 × 6 cm, and covered by a black fusion crust. A mass of 67 g was donated to Museu Nacional/UFRJ and is housed at the Department of Geology and Paleontology (Inventory number 142 MT). In hand specimen, it shows a grayish interior with some slightly reddish-brown spots due to weathering, also visible in thin-section. Metal shows very few weathering suggesting that the recovery was done shortly after the fall (Fig. 1). In this paper a detailed petrographic, chemical and Mössbauer spectroscopy study of this new meteorite is reported.

## 2 Materials and Methods

Four polished thin-sections were etched with 2% nital to reveal the metallographic microstructures and studied using optical, scanning electron microscopy (SEM) electron microprobe and Mössbauer spectroscopy. Optical microscopy was performed by transmitted and reflected light, using a Petrographic Microscope Carl Zeiss, with Axionvision Release 4.7 software. The electron microscopy was performed by back-scattering electron imaging (BSEi) on a Digital Scanning Microscope, (DSM 940A Zeiss), equipped with a system for energy-dispersive X-ray micro-analysis (LINK/Oxford-exLII).

Major element chemical compositions were obtained by an ARL-SEMQ (WDS) electron microprobe with analyses acquired at conditions of 15 kV acceleration potential and 15 nA sample currents. Estimated precision for major and minor elements is better than 3%


**Fig. 1** Panoramic photomicrograph in plane transmitted light of the whole thin-section, showing the distribution of objects

and for Na about 10%. Natural and synthetic standards were used for calibration and an online ZAF correction was applied to the data.

The $^{57}$Fe Mössbauer spectroscopy ($^{57}$Fe-MS) experiments were performed at room temperature in standard transmission geometry, using a 25 mCi $^{57}$Co/Rh radioactive source in sinusoidal mode. The NORMOS code was used for the spectrum analysis.

## 2.1 Petrography

### *2.1.1 Texture*

Under optical inspection, Lavras do Sul shows a texture that is similar to other equilibrated ordinary chondrites. Both matrix and chondrules have undergone considerable recrystallization.

The chondrules are embedded in a recrystallized and clastic matrix with most grains ranging in size between 50 and 150 μm and down to the limits of microscopic resolution. There are patchy areas with different colors and veins of secondary minerals (mainly iddingsite) that crosscut the matrix. Some chondrules show a poorly defined interface between the chondrules and matrix, in particular some radial and barred chondrules with irregular boundaries. Metal grains and troilite are scattered through the matrix as well as in the chondrules.

### *2.1.2 The Chondrules*

The chondrules in Lavras do Sul are mainly poorly defined, although some show distinct outlines, particularly when viewed under crossed polarized transmitted and reflected light (Fig. 2). The chondrules are more or less rounded in outline, irregular or fragmented. Chondrules range in apparent diameter between 200 and 2,000 μm, with three average population sizes: small (~300 μm), medium (~700 μm) and large (~1,700 μm). Here, the size frequency and apparent dimensions of chondrules measured in thin-sections were determined by a combination of measurement techniques (Eisenhour 1996; King and King 1978). Chondrules with non-porphyritic and porphyritic textures are observed, including: Barred Olivine (BO), Radial Pyroxene (RP), Granular olivine-pyroxene (GOP), Porphyritic olivine-pyroxene (POP), Microcrystalline chondrule and a Chromite-rich chondrule.

Barred olivine (BO) chondrules range in size between 500 and 1,200 μm in apparent diameter. In most of them the olivine bars as well as the rims occur in parallel orientation (e.g., showing simultaneous extinction under cross-polarized transmitted light) suggestive of a single crystal. Some of these objects are bounded by a rim of olivine. The bars of the defined chondrules vary widely in size from 18 to 20 μm up to 80 to 120 μm (the latter measured in a fragment of a BO). The skeletal crystals of olivine commonly are associated with interstitial aggregates of orthopyroxene. The mesostasis is most glassy, with incipient recrystallization with microcrystalline thin pyroxene bars (Fig. 2b)

Radial Pyroxene (RP) chondrules are less common than those of the Barred Olivine type, having sizes varying from 500 to 900 μm with a sub-rounded shape. They have thin lamellae of pyroxene with a radiating fan distribution as a result of an eccentric nucleation point near the surface. The main mineral is orthopyroxene, with fine lamellae of clino-pyroxene. In some of these objects euhedral skeletal olivine grains were observed.

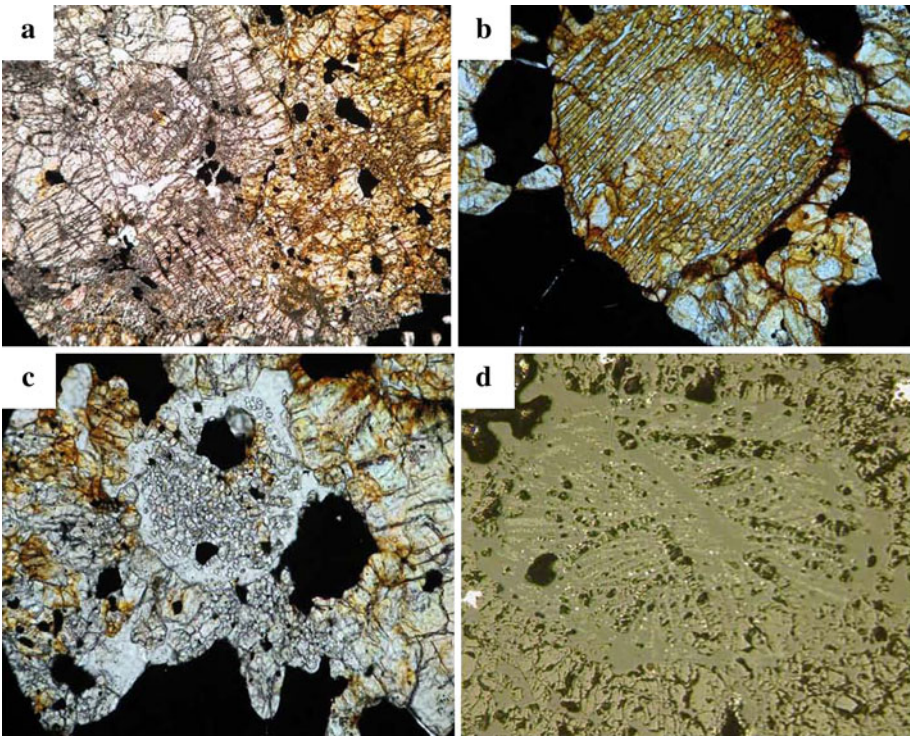


**Fig. 2** **a** Photomicrograph of Lavras do Sul meteorite in plane polarized transmitted light showing the chondritic texture with chondrules poorly defined. Length of the field: 5.2 mm. **b** Plane transmitted light photomicrographs showing a barred olivine chondrule with their unmistakable texture composed of one set of elongated parallel bars of olivine with a glassy mesostasis between *bars*. Length of the field: 1.3 mm. **c** Plane polarized transmitted light photomicrographs of microcrystalline chondrule showing anhedrals small crystals of olivine and pyroxene in a glassy mesostasis. **d** Photomicrographs in reflected light showing a chromite-rich chondrule (600 μm in apparent diameter), composed of large olivine bars and glass. Immersed in the Na-rich glassy mesostasis there are small euhedral olivine crystals and euhedral chromite crystals

Granular olivine-pyroxene chondrules (GOP) have sizes varying from 500 to 600 μm. The anhedral crystals of olivine and pyroxene have sizes around 25 μm in a recrystallized mesostasis.

Porphyritic olivine-pyroxene chondrules (POP) are the largest objects, with a size range from 700 to 1,900 μm. They are composed of large euhedral to subhedral olivine or pyroxene crystals with interstitial aggregates of pyroxene and sometime plagioclase. They have sizes up to 1,800 μm and are immersed in a slightly devitrified glassy mesostasis sometimes are surrounded by large opaque minerals. Crystals show undulatory extinction, planar structure and numerous cracks sometimes filled with iddingsite.

Microcrystalline chondrules have sizes around 700 μm with anhedral small crystals of olivine and pyroxene in a recrystallized mesostasis.

Among the different types of chondrules described above, one particular object has called attention. It is a chromite-rich chondrule (600 μm in apparent diameter) composed of large olivine bars and glass (Fig. 2d). Immersed in the Na-rich glass there are small euhedral olivine crystals and euhedral chromite crystals that contribute to the dark aspect of the object in transmitted light.

## 2.2 Mineral Chemistry

### *2.2.1 Major Element Phase Compositions*

Representative and averaged electron microprobe analyses (EMPA) of the phases are given in Tables 1, 2, 3, 4, 5, 6 and 7. Olivine ($Fa_{24,\ 9}$) typically has FeO contents between 22.1 and 23.4 wt% (Table 1). The MnO and CaO contents vary between (0.65–0.77 wt%) and (0.02–to 0.07 wt%), respectively. Pyroxenes are low-Ca pyroxene ($Fs_{22.6}$) with FeO contents varying from 13.8 to 14.5 wt% (Table 2), $TiO_2$ and CaO in the range of 0.11–0.27 wt% and 0.70–0.97 wt%, respectively, with $Cr_2O_3$ from 0.07 to 0.13 wt%. Na and K are mostly below the detection limit of the electron microprobe. In the chromite-rich chondrule, the composition of the large and small euhedral olivine crystals show no significant variation in their major elements. Small euhedral chromites in the mesostasis have $TiO_2$, $Al_2O_3$ and MgO contents around 4.3, 6.0 and 3.7 wt%, respectively. The glassy mesostasis is rich in $Na_2O$ and $K_2O$ ($\sim$2 and 1 wt%, respectively). Representative analyses of the different phases are shown in Table 3.

### *2.2.2 Accessory Minerals*

In order of decreasing abundance the accessory minerals are: troilite, kamacite, taenite, plagioclase, chromite and magnetite.

Plagioclase occurs as tiny anhedral crystals, occasionally showing twinning. However, most of them are transformed into maskelynite, ranging in size from 5 to 123 μm (the majority of the grains are <50 μm) (Table 4).

**Table 1** Representative EMP analysis of olivine (wt%)

| | | | | | | | | |
|---|---|---|---|---|---|---|---|---|
| $SiO_2$ | 38.4 | 38.2 | 38.4 | 37.7 | 38.5 | 38.0 | 38.6 | 39.2 |
| $TiO_2$ | 0.05 | | 0.04 | 0.05 | 0.05 | 0.05 | | 0.02 |
| FeO | 22.7 | 22.7 | 22.9 | 23.4 | 22.4 | 22.1 | 22.7 | 22.5 |
| MnO | 0.68 | 0.65 | 0.74 | 0.74 | 0.77 | 0.68 | 0.71 | 0.65 |
| MgO | 38.4 | 37.7 | 38.6 | 37.7 | 38.2 | 39.0 | 37.9 | 38.0 |
| CaO | | 0.02 | 0.06 | 0.06 | 0.05 | 0.04 | 0.07 | |
| Total | 100.2 | 99.2 | 100.8 | 99.7 | 100.0 | 99.9 | 100.0 | 100.3 |

**Table 2** Representative EMP analysis of pyroxene (wt%)

| | | | | | | | | |
|---|---|---|---|---|---|---|---|---|
| $SiO_2$ | 55.4 | 54.8 | 54.8 | 55.2 | 56.0 | 55.6 | 55.3 | 55.6 |
| $TiO_2$ | 0.19 | 0.11 | 0.23 | 0.22 | 0.22 | 0.27 | 0.23 | 0.27 |
| $Al_2O_3$ | 0.19 | 0.15 | | | | | | |
| $Cr_2O_3$ | 0.11 | 0.09 | 0.04 | 0.11 | 0.13 | 0.07 | 0.13 | 0.09 |
| FeO | 14.1 | 13.9 | 14.5 | 14.3 | 14.2 | 14.5 | 14.0 | 13.8 |
| MnO | 0.67 | 0.79 | 0.55 | 0.74 | 0.76 | 0.74 | 0.67 | 0.74 |
| MgO | 28.5 | 28.3 | 28.6 | 29.0 | 28.7 | 28.7 | 28.6 | 28.6 |
| CaO | 0.82 | 0.97 | 0.79 | 0.99 | 0.80 | 0.74 | 0.93 | 0.70 |
| Total | 100.0 | 99.1 | 99.5 | 100.6 | 100.8 | 100.6 | 99.9 | 99.8 |

**Table 3** EMP analysis of the olivine-chromite-rich chondrule (wt%)

| | Ol (B) | Ol (B) | Ol (euh) | Ol (euh) | Chromite | Chromite | Chromite | Glass | Glass |
|---|---|---|---|---|---|---|---|---|---|
| $SiO_2$ | 36.4 | 39.4 | 39.7 | 39.8 | 0.50 | 0.53 | 0.64 | 68.5 | 68.1 |
| $TiO_2$ | 0.07 | 0.07 | 0.00 | 0.00 | 4.47 | 4.29 | 4.24 | 0.00 | 0.07 |
| $Al_2O_3$ | 0.42 | 0.06 | 0.25 | 0.14 | 5.99 | 5.97 | 6.13 | 25.3 | 25.2 |
| $Cr_2O_3$ | 0.50 | 0.46 | 0.31 | 0.46 | 53.7 | 53.6 | 53.3 | 0.33 | 0.00 |
| FeO | 29.8 | 22.6 | 21.8 | 22.0 | 30.7 | 30.9 | 31.8 | 0.37 | 0.52 |
| MnO | 0.34 | 0.38 | 0.51 | 0.47 | 0.48 | 0.60 | 0.64 | 0.04 | 0.04 |
| MgO | 32.2 | 36.9 | 35.3 | 35.8 | 3.61 | 3.81 | 3.56 | 0.02 | 0.02 |
| CaO | 0.11 | 0.02 | 0.05 | 0.02 | 0.07 | | 0.05 | 2.40 | 2.13 |
| $Na_2O$ | | | | | | | | 2.21 | 2.70 |
| $K_2O$ | | | | | | | | 1.03 | 1.07 |
| Total | 99.8 | 99.8 | 98.0 | 98.7 | 99.4 | 99.7 | 100.3 | 100.2 | 99.9 |

*Note Ol (B)*, large olivine bar; *Ol (euh)*, small euhedral olivines present in the glass

**Table 4** Representative EMP analysis of plagioclase (wt%)

| | | | | | |
|---|---|---|---|---|---|
| $SiO_2$ | 67.0 | 67.9 | 65.9 | 65.8 | 67.5 |
| $TiO_2$ | 0.07 | 0.04 | 0.05 | 0.04 | 0.00 |
| $Al_2O_3$ | 22.1 | 21.7 | 21.3 | 21.7 | 22.1 |
| $Cr_2O_3$ | | | 0.03 | | 0.07 |
| FeO | 0.45 | 0.58 | 0.36 | 0.36 | 0.75 |
| CaO | 2.09 | 2.12 | 2.15 | 2.14 | 2.12 |
| $Na_2O$ | 7.84 | 6.82 | 8.02 | 7.52 | 6.90 |
| $K_2O$ | 0.90 | 1.35 | 1.32 | 1.20 | 1.11 |
| Total | 100.5 | 100.6 | 99.2 | 98.8 | 100.5 |
| Ab | 81.8 | 76.8 | 79.6 | 79.2 | 78.4 |
| An | 12 | 13.2 | 11.8 | 12.5 | 13.3 |
| Or | 6.2 | 10 | 8.6 | 8.3 | 8.3 |

**Table 5** Representative analysis of Troilite (wt%)

| | | | | | |
|---|---|---|---|---|---|
| Fe | 61.6 | 61.2 | 62.0 | 62.8 | 62.8 |
| Ni | 2.86 | 1.10 | 0.05 | 0.09 | 0.44 |
| S | 36.5 | 37.6 | 38.4 | 37.8 | 37.7 |
| Total | 100.9 | 100.1 | 100.5 | 100.7 | 100.9 |

Troilite is very abundant, comprising about 60% of the opaque minerals. It is commonly observed surrounding large chondrules, but can also occur isolated or associated with metal. Several large troilite crystals exhibit well developed polycrystalline grains with 120° intersections (triple junctions). Representative analyses are given in Table 5.

Metal grains are typically irregular in shape; some are elongated, others subhedral (Fig. 3). They are less abundant than troilite and some grains are composed of kamacite and taenite. In etched samples the taenite shows a cloudy core and a tetrataenite rim that can reach 1–3 μm thick (Fig. 3b). Under optical microscopy the cloudy core is seen to be composed of tetrataenite and sometimes martensite. A compositional profile (P1, Fig. 3a)

**Table 6** Representative analysis in metal (P1) (wt%)

| | | | | | T | | | | | T | T | | |
|---|---|---|---|---|---|---|---|---|---|---|---|---|---|
| Fe | 93.6 | 93.6 | 93.5 | 92.9 | 51.9 | 80.4 | 80.2 | 81.3 | 80.5 | 50.6 | 49.4 | 92.0 | 92.0 |
| Ni | 6.4 | 6.4 | 6.0 | 6.5 | 44.7 | 19.5 | 19.5 | 17.8 | 19.0 | 50.1 | 50.2 | 6.5 | 6.8 |
| Co | 0.62 | 0.60 | 0.58 | 0.63 | 0.08 | 0.55 | 0.51 | 0.62 | 0.53 | 0.04 | 0.03 | 0.55 | 0.57 |
| Total | 100.7 | 100.7 | 100.1 | 100.1 | 96.8 | 100.5 | 100.3 | 99.8 | 100.1 | 100.8 | 99.6 | 99.2 | 99.4 |

T=Tetrataenite regions

**Table 7** Representative analysis in metal vein (P2) (wt%)

| | | | | | |
|---|---|---|---|---|---|
| Fe | 93.1 | 93.1 | 93.3 | 93.3 | 93.2 |
| Ni | 6.8 | 6.6 | 6.5 | 6.6 | 6.8 |
| Co | 0.93 | 0.94 | 0.92 | 0.90 | 0.90 |
| Total | 100.9 | 100.6 | 100.7 | 100.9 | 100.9 |

performed near the edge of a large metal grain included in troilite shows the high variation in Ni contents in kamacite, tetrataenite and cloudy taenite (Table 6, Fig. 4). Kamacite (α nickel–iron, b.c.c) grains are polycrystalline and exhibits Neumann lines, shock-produced twin lamellae, and sometimes displays Widmanstätten-like patterns. Individual kamacite appears commonly with irregular shapes either isolated or associated with troilite. Kamacite can also form large veins ($\sim$7 mm $\times$ 1 mm), that are observed crosscutting a thin-section (Fig. 3c). The kamacite crystals show irregular borders towards the silicates. A step profile, performed across the vein, indicates that the chemical composition (e.g., Ni content) is quite constant (P2, Fig. 3c, Table 7). Metal can also develop zoneless plessite texture as pearlitic plessite (Sears and Axon 1975), composed of roughly equal parts of kamacite and taenite (Table 8, Fig. 3d–f).

Small FeNi metal spherical within silicate melt pockets and veins (Sears and Dodd 1998) are also observed. Magnetite appears associated with troilite and is poikilitic in the silicate phases. Occasionally silicate minerals (e.g., olivine, pyroxenes, plagioclase) occur as inclusions in metal. Chromite occurs as subhedral to euhedral unzoned crystals, associated with silicate phases.

The Mössbauer analysis of the Lavras do Sul bulk sample showed a spectrum composed of overlapping paramagnetic and magnetic phases. The spectra at room temperature exhibit two $Fe^{2+}$ doublets attributed to olivine and pyroxene, and additionally two magnetic phases associated to Fe–Ni phases (kamacite and taenite) and troilite. The Mössbauer spectrum of the metal particles extracted from the bulk sample (Fig. 5), free of silicates and troilite, exhibits only kamacite and small amounts of the intergrowth tetrataenite/antitaenite (Rancourt and Scorzelli 1995).

### *2.2.3 Secondary Minerals*

The products of terrestrial weathering are iron oxide hematite ($Fe_2O_3$) and hydrated iron oxide minerals as iddingsite, goethite, lepidocrocite and others. These products are generally fine-grained and intimately mixed. In Lavras do Sul, iddingsite fills fractures and veins and tarnishes the silicate minerals with reddish and yellowish colors. Metal, however, is relatively fresh with only few weathering features, suggesting a recovery shortly after the fall.

## 3 Discussions and Conclusions

Lavras do Sul consists of chemically homogeneous major (and minor) phases (e.g., Tables 1, 2), with plagioclase showing a uniform composition (Table 4). The progressive stages of shock metamorphism in ordinary chondrites (Stöffler et al. 1991) are mainly based on shock effects in olivine and plagioclase. The presence of deformation features such as planar fractures and undulatory extinction in plagioclase and olivine, with fractures in most silicate grains, determine the shock stage as S3.

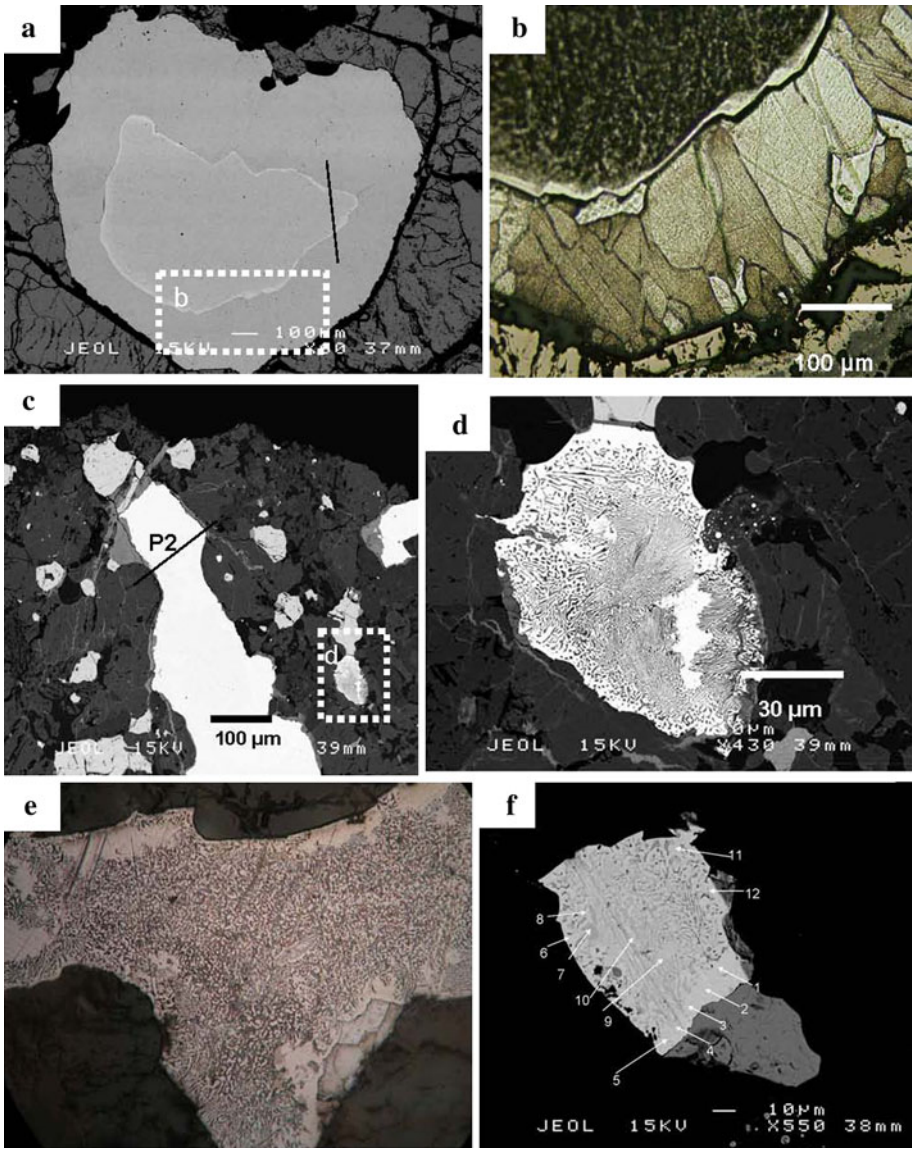


**Fig. 3** **a** BSE image of kamacite with cloudy taenite inside bordered by tetrataenite. *Dark line* indicates location of the profile P1 (Table 6). The *white rectangle* in *dotted line* shows the location of **b**. **b** Reflected light photomicrograph showing the aspect of phases after being etched by nital 2%. The cloudy taenite (*black*) is bordered by tetrataenite *(bright silver*) and surrounding by polycrystalline kamacite. **c** Reflected light photomicrograph showing a metal vein. *Black line* indicates profile P2 (Table 7). The *white rectangle* in *dotted line* shows the location of **d**. **d** BSE image of metal with plessitic texture composed of roughly equal parts of kamacite and taenite. **e** Reflected light photomicrograph showing metal with plessitic texture, Length of the field 2.6 mm. **f** BSE image of metal. *Numbers* indicate location of the EMP analysis (Table 8)

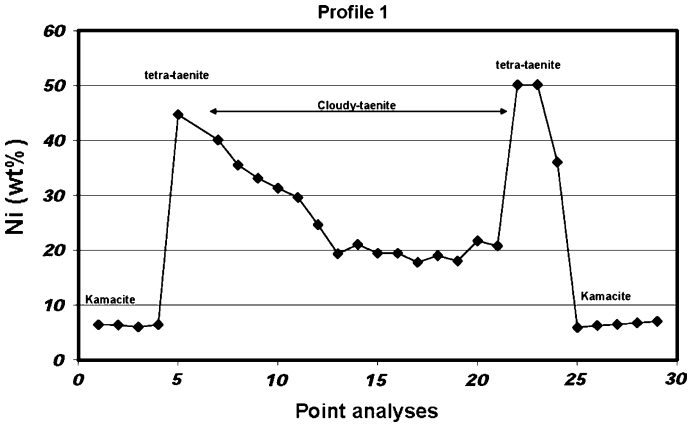


**Fig. 4** Point step profile showing the classical M shape in the Ni contents of P1 (see Fig. 3a)

**Table 8** EMP analysis of a metal grain with plessitic texture

| | 1 | 2 | 3 | 4 | 5 | 6 | 7 | 8 | 9 | 10 | 11 | 12 |
|---|---|---|---|---|---|---|---|---|---|---|---|---|
| Fe | 46.9 | 47.3 | 50.1 | 48.2 | 48.0 | 67.1 | 92.1 | 68.8 | 69.0 | 69.6 | 92.5 | 69.7 |
| Ni | 53.0 | 52.7 | 50.5 | 51.2 | 52.2 | 31.2 | 5.4 | 30.5 | 29.3 | 29.7 | 5.6 | 29.7 |
| Co | 0.05 | 0.16 | 0.12 | 0.08 | 0.04 | 0.37 | 0.61 | 0.27 | 0.25 | 0.26 | 0.49 | 0.34 |
| Total | 100.1 | 100.3 | 100.7 | 99.6 | 100.3 | 98.8 | 98.3 | 99.7 | 98.6 | 99.5 | 98.6 | 99.8 |

Homogenous plagioclase—such as those observed in Lavras do Sul—should, however, be expected in unshocked ordinary chondrites. But, because of the slow diffusion rates of NaSi-CaAl substitutions (Hart 1981), uniform compositions can also be expected in highly shocked chondrites.

The presence of ambiguous features indicating different shock stages in the same chondrite is not uncommon, and could point towards shock and subsequent post-shock annealing, that could preserve features normally associated with high degrees of shock metamorphism. Shock metamorphic effects can be partially removed by annealing resulting in a shock classification that could be lower than the maximum stage experienced by the chondrite.

Troilite appears to be a sensitive indicator of shock (Bennett and McSween 1996); it becomes polycrystalline with 120° triple junctions with shock loading between 35 and 60 GPa. This corresponds to a peak pressure much higher (e.g., S4: 20–35 GPA, S5: 35–55 GPA) than those estimated based in shock effects in olivine and plagioclase (S3).

Zoneless plessite is common in type 5 and 6 low shock chondrites (S1–S2) (Bennett and McSween 1996). Also pearlitic plessite is only observed in L chondrites of low shock stage below S4 (Sears and Axon 1975). However, Stöffler et al. (1991) suggest that the presence of coarse-grained pearlitic plessite could be interpreted as having been formed by a post-shock annealing after the chondrite was affected by a high shock stage above S4.

Metal is a phase that should be easier to equilibrate than all other phases, but is commonly not equilibrated. The presence of melt pockets indicates temperatures >800°C (e.g., partial or in situ melting above 950°C (Sears and Axon 1975) and this should have homogenized all metal grains. In such a scenario kamacite and taenite might produce

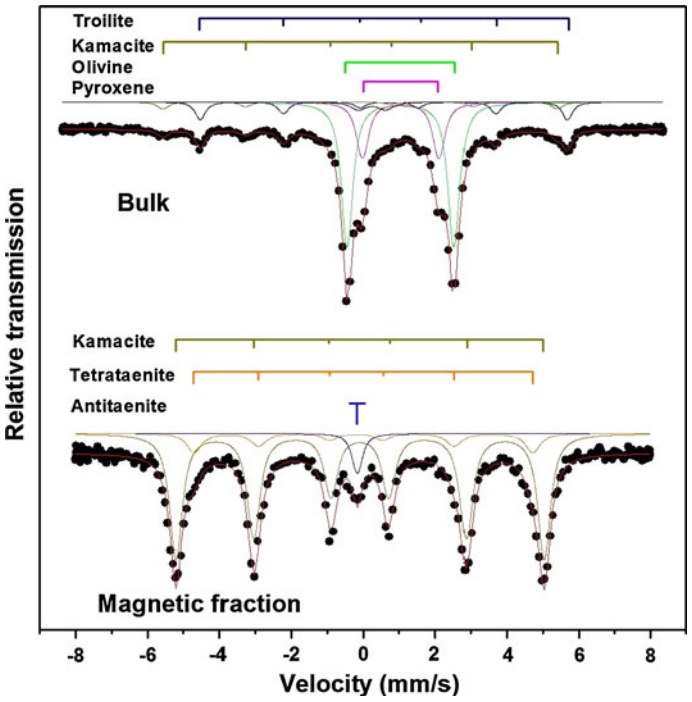


**Fig. 5** The $^{57}$Fe Mössbauer spectra performed at room temperature, the bulk sample shows kamacite, troilite, olivine and pyroxene; after magnetic separation it shows kamacite, tetrataenite and antitaenite

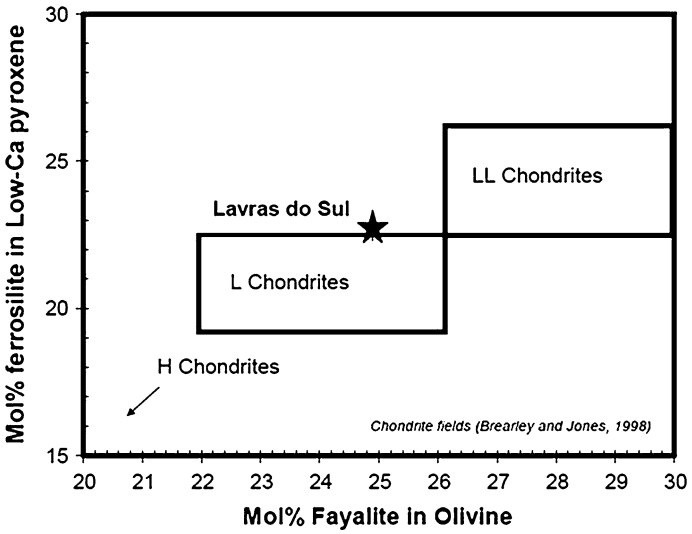


**Fig. 6** Classification of Lavras do Sul considering the average of Low-Ca pyroxene and olivine. Chondrites fields from Brearley and Jones (1998)

composite grains with equal amount of both phases. This is rarely observed in chondrites (Urey and Mayeda 1959) as well as in Lavras. The zoned taenite grains with tetrataenite and cloudy taenite core with the classical "M" shaped Ni profile (Fig. 4) are interpreted to be the result of diffusion-controlled transformation taenite → taenite + kamacite during very slow cooling (Heymann 1967). This indicates that Lavras do Sul had a variable metallographic cooling rate. This result is in agreement with previous work (Willis and Goldstein 1983) that shows that metallographic cooling rates are rarely unique in a given chondrite.

The new Brazilian meteorite, Lavras do Sul, is thus classified as an ordinary chondrite (L5) (Van Schmus and Wood 1967; Rubin 1990) (Fig. 6) with shock stage S3 (Stöffler et al. 1991) and a degree of weathering W1 (Wlotzka 1993).

**Acknowledgments** E. Zucolotto acknowledges FAPERJ for financial support. M.E. Varela is greatful to Agencia PICT 212 and CNPq for financial support during scientific visits to CBPF. R.B. Scorzelli would like to thank FAPERJ and CNPq for financial support; P. Munayco and E. dos Santos are grateful to FAPERJ and CAPES and L. L. Antonello to CBPF/MCT for their fellowships.

## References

M.E. Bennett, H.Y. Jr. McSween, Meteorit. Planet. Sci. **31**, 783–792 (1996)
A.J. Brearley, R.H. Jones, Chondritic meteorites, in *Planetary Materials,* ed. by J.J. Papike (Mineralogical Society of America, Washington D.C., 1998), pp. 3-1–3-398
D.D. Eisenhour, Meteorit. Planet. Sci. **31**, 243–248 (1996)
S.R. Hart, Geochimica Cosmochimica Acta **45**, 279–291 (1981)
D. Heymann, Icarus **6**, 189–221 (1967)
T.V.V. King, E.A. King, Meteoritics **31**, 47–72 (1978)
D.G. Rancourt, R.B. Scorzelli, J. Magn. Magn. Mater. **150**, 30–36 (1995)
A.E. Rubin, Geochimica et Cosmochimica Acta **54**, 1217–1232 (1990). H.Y. Jr.
D.W.G. Sears, H.J. Axon, Meteoritics **10**, 486–487 (1975)
D.W.G. Sears, R. T. Dodd, in *Meteorites and the Early Solar System*, ed. by J.F. Kerridge, M.S. Matthews (University of Arizona Press, Tucson, AZ, 1998), pp. 3–31
D. Stöffler, K. Keil, E.R.D. Scott, Geochim. Cosmochim. Acta **55**, 3845–3867 (1991)
H.C. Urey, T. Mayeda, Geochim. Cosmochim. Acta **17**(1–2), 113–116 (1959)
W.R. Van Schmus, J.A. Wood, Geochimica et Cosmochimica Act **31**, 747–765 (1967)
J. Willis, J.I.Goldstein, in *14th Lunar & Planetary Science Conference*. J. Geophys. Res. Suppl. **88**, B 287–B 292 (1983)
F. Wlotzka, Meteoritics **28**, 460 (1993)